11th U.S. National Combustion Meeting
Organized by the Western States Section of the Combustion Institute
March 24–27, 2019
Pasadena, California

Enabling Tailored Porous Media Burners via Additive Manufacturing

Sadaf Sobhani[1*], *Priyanka Muhunthan*[1], *Danyal Mohaddes*[1], *Emeric Boigne*[1], *Zhilong Cheng*[1], *and Matthias Ihme*[1]

[1]*Department of Mechanical Engineering, Stanford University, Stanford, CA 94305*
[*]*Corresponding author:* ssobhani@stanford.edu

Abstract: Compared to conventional free-flame systems, Porous Media Burners (PMBs) are characterized by significantly higher burning velocities, enhanced flame stabilization, and lower emissions of nitric oxides. Current PMB implementations utilize a two-zone concept in which the flame stabilizes at the interface between two porous matrices of different topologies. In this work, the feasibility of additive manufactured PMBs with spatially graded porous matrices is experimentally investigated. Topology gradation was recently proposed and shown to result in a significant enhancement of the power-dynamic range and approximately 50% higher blow-off limits compared to conventional two-zone designs. In the current study, smoothly graded porous matrices are designed and manufactured using lithography-based ceramic manufacturing, thus demonstrating the potential for tailoring PMBs for enhanced performance.
Keywords: ***Porous media combustion, Additive manufacturing, Lithography-based ceramic manufacturing***

1. Introduction

Porous Media Burners (PMBs) enable enhanced combustion properties by internally recirculating heat released from the combustion products upstream to the reactants via an inert solid matrix. Due to their high porosities and consequently low pressure drops, reticulated ceramic foams are some of the most commonly used materials in PMBs. Such foams are currently manufactured using the replication of polymer foams by coating with a ceramic slurry or chemical vapor deposition [1]. The replication method, and other traditional manufacturing techniques, are used to produce foams of constant pore diameter and porosity, which can then be stacked and sintered together to create a step-wise graded part.

In conventional PMBs, the flame is anchored at the interface of two porous materials, which are designed to quench the flame from propagating upstream [2]. This design is referred to as a two-zone interface-stabilized —or step —PMB. Recently, a new functionally graded PMB design was proposed [3], where the gradation in topology (i.e. porosity, pore diameter, cell diameter, etc.) enables a continuous variation of the local Stanton number and optical depth, allowing the flame to stabilize dynamically within the porous matrix and for a wider range of operating conditions. Through theoretical and computational analysis of the performance of functionally graded PMBs, followed by experiments using step-wise graded porous media, it was shown that the proposed physical design of the solid medium results in a significant enhancement of the power-dynamic

range and approximately 50% higher blow-off limits compared to the two-zone designs. These results indicate that properties of PMBs, such as flame stability, can be optimized by tailoring the underlying porous structure. However, due to limitations in conventional porous matrix manufacturing technologies, matrix properties such as pore diameter and porosity cannot be varied independently, hindering the ability to systematically study their effects on PMB performance.

Enabling such tailoring capabilities for optimizing PMB performance necessitates the use of advanced manufacturing techniques beyond the traditional replication method. Additive Manufacturing (AM) allows for the fabrication of highly complex and customized structures on a layer-by-layer basis from Computer Aided Design (CAD) model data. The current AM methods applicable to ceramic parts are divided into direct and indirect techniques [4]. Direct techniques are powder-based and use thermal energy input by a laser to selectively melt or sinter the ceramic grains to form the final part (i.e. selective laser sintering/melting). In contrast, indirect techniques first print a "green part" consisting of the ceramic particles and an organic binder, which is then thermally treated to remove the organic components and sinter the ceramic grains. Lithography-based methods are a subset of indirect techniques that rely on selective space-resolved exposure to light to solidify the liquid suspension. In Digital Light Processing (DLP), a part is created from a suspension of ceramic particles in a photosenstive resin, which is shaped via photochemical reactions. A photopolymerization-based technology, such as DLP, enables higher feature resolution and surface quality as compared to thermal energy-based methods such as selective laser sintering [5].

In the present study, DLP is used to perform Lithography-based Ceramic Manufacturing (LCM) to demonstrate the fabrication of functionally graded matrix structures, which are predicted to have advantageous combustion properties as compared to conventionally employed two-zone PMBs. The matrix topology used as the input to the LCM is designed using periodic surface equations. Lastly, the manufactured samples are implemented in a PMB and tested over a range of operating conditions to test the feasibility and performance of AM materials in PMBs.

2. Mathematically-defined graded porous structure

With the goal of manufacturing a smoothly graded PMB, the first step is to generate the topology of a functionally graded porous structure. The matrix unit type used in this study is based on a subset of periodic surface equations, known as Triply Periodic Minimal Surfaces (TPMS). TPMS offer several advantages over strut-based lattice structures (i.e. body-centered-cubic), including high surface-to-volume ratio, enhanced pore connectivity, and ease of functional grading [6]. TPMS are commonly used in biomedical applications for tissue and bone engineering [6–10].

The topologically simplest forms of TPMS that have cubic lattice symmetry are the primitive (P), gyroid (G) and diamond (D) surfaces [11, 12], which are illustrated in Fig. 1. These surfaces are characterized by interconnectivity order, which quantifies the number of struts at each node of the lattice. P, D, and G surfaces have an interconnectivity order of 6, 4 and 3, respectively. In this study, D surfaces are used to create lattice structures similar to porous foams typically used in PMBs. The D surface is expressed using the following equation:

$$F(x,y,z) = sin(\omega x)sin(\omega y)sin(\omega z) + sin(\omega x)cos(\omega y)cos(\omega z) + cos(\omega x)sin(\omega y)cos(\omega z) + cos(\omega x)cos(\omega y)sin(\omega z) + q, \quad (1)$$

where ω and q control the pore density (e.g. pore size) and porosity, respectively. The $F = 0$ isosurface is treated as a boundary separating solid and void regions of a three-dimensional

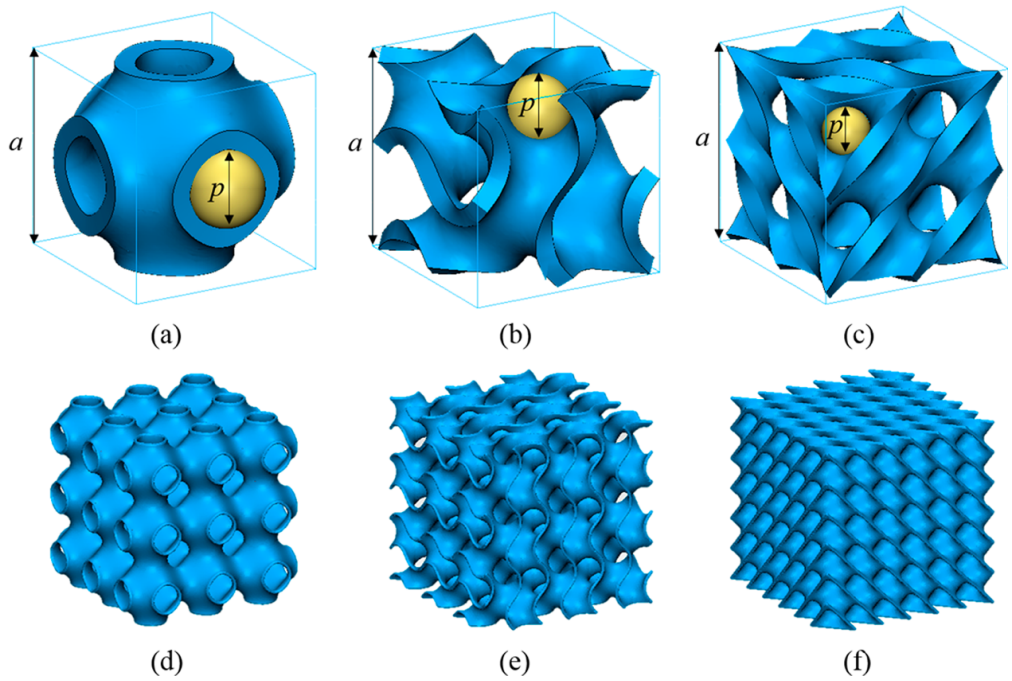

Figure 1: TPMS unit cells (a-c) and corresponding 3 x 3 x 3 repeated unit cells (d-f), where (a) and (d) are P surfaces, (b) and (e) are G surfaces, and (c) and (f) are D surfaces, each with unit cell size and pore size labeled by a and p, respectively. Figure from Vijayavenkataraman et al. [10].

structure. Regions where F ≤ 0 is defined to be solid and regions where F > 0 is void space. To facilitate lattice functional grading of porosity and pore size, Eq. 1 is adjusted such that either ω and/or q are replaced by spatially-dependent parameters. In the current study, the following functions were used to generate a linear grading in the axial direction:

$$q(z) = q_1 + \frac{(q_2 - q_1)z}{H}, \tag{2a}$$

$$\omega(z) = \omega_1 + \frac{(\omega_2 - \omega_1)z}{H}, \tag{2b}$$

where H is the height of the sample, and subscripts 1 and 2 refer to the limits of the parameter within the sample. These parameter limits are first determined from the desired limits of porosity and pore size. Figure 2 illustrates increasing degrees of porosity gradation by varying the q_1 and q_2. Once the desired geometry is modeled, an isosurface is created and converted to a stereolithography (STL) file for input to the printer system, using the mathematical modeling software MathMod.

3. Experimental Setup

The porous samples designed and converted to STL files were sent to Lithoz GmbH for printing using LCM technology. Green parts were first manufactured with DLP using a photocurable alumina

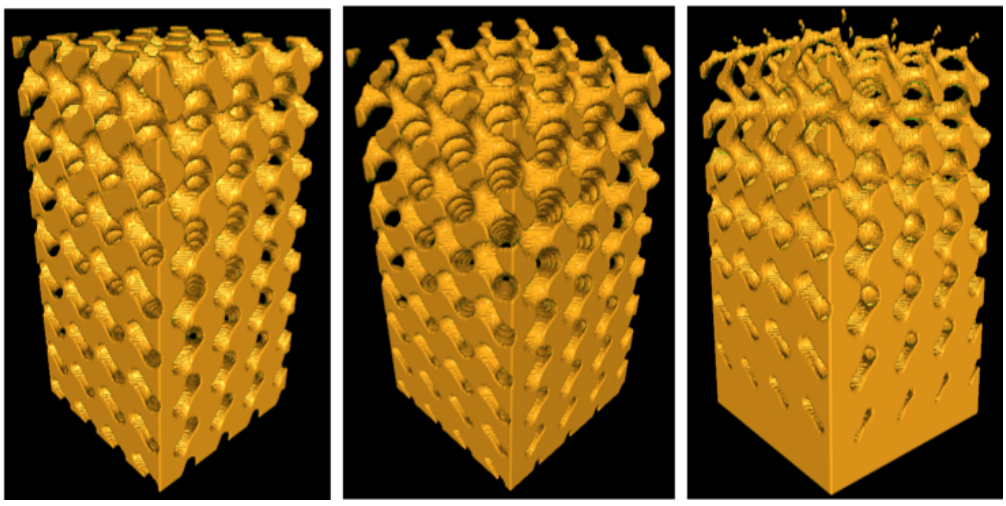

Figure 2: From left to right, increasing degrees of porosity gradation.

(Al_2O_3) suspension. After thermal post-processing to remove the organic binder, the resulting alumina product has a purity of 99.8% and a material porosity of 1.6% (see Fig. 3).

The burners tested consisted of AM alumina porous structures with different pore size, porosity, and gradation profiles, outlined in Table 1. Burner A is graded in porosity and constant in pore diameter profile, and conversely, Burner B is graded in pore diameter and constant in porosity. The pore diameter and porosity profiles tested were based on previous computational work [3]. The porous samples were wrapped in insulation and housed in a quartz tube (see Fig. 3). All experiments were performed using a methane/air mixture at atmospheric pressure. Flow rates of reactants were measured and controlled using Alicat Scientific mass flow controllers (refer to [3] for further details). Compressed air and methane flows were mixed at a tee-junction approximately 200 tube diameters upstream of the burner to achieve a homogeneous mixture prior to entry into the burner.

Burner A	**Burner B**
graded porosity	graded pore diameter
$d = 2.5$ mm	$d = 1.5$-3.5 mm
$\varepsilon = 65$-85%	$\varepsilon = 75\%$
$H = 75$ mm	$H = 75$ mm
$D = 20$ mm	$D = 20$ mm

Table 1: Geometric parameters for the burners tested, where d, ε, H, and D refer to pore diameter, porosity, burner height, and burner diameter, respectively.

Six K-type mineral-insulated thermocouples were placed along the axial profile of the burner at azimuthal locations varying by 60°. Temperature measurements were primarily used to determine flame location and stability. Stable operation was defined as continuous operation without changes in thermocouple measurements greater than 5 K over 5 minutes. After each stable operating condition was determined, the mass flux was changed to find the maximum stable flow rate for each

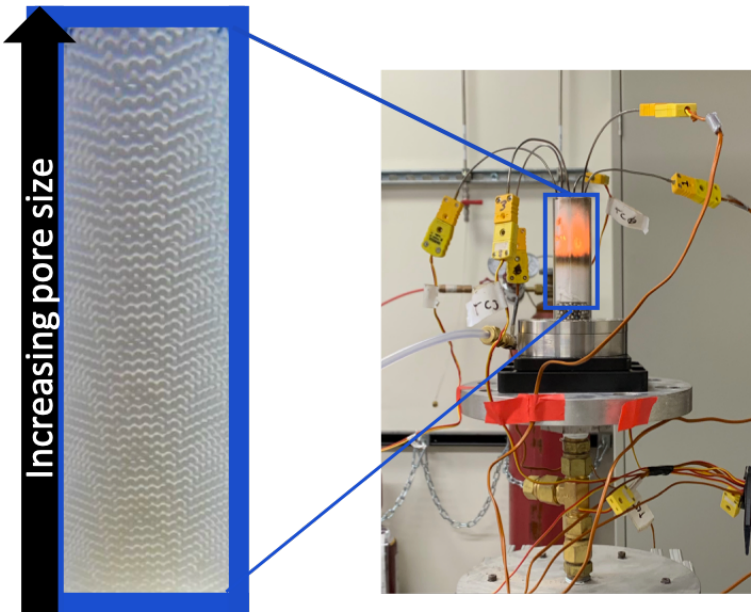

Figure 3: (Left) Porous structure with graded pore diameter ($d = 1.5$-3.5 mm) and constant porosity (75%) profile after binder burnout and sintering of green part. (Right) Experimental setup illustrating the burner in operation with instrumented thermocouples. Methane/air flows from bottom to top, and the flame is visible through the insulation and quartz tube.

equivalence ratio. The blow-off limit was determined first by the occurrence of the maximum temperature measurement at the thermocouple furthest downstream, and subsequently by the continual decrease in temperature measured by this thermocouple. Flashback was determined similarly, except that the maximum temperature was observed at the thermocouple furthest upstream, followed by a decrease in temperature of its adjacent thermocouple.

4. Results and Discussion

Flame stability measurements are presented for the two burners outlined in Table 1. At each air-fuel equivalence ratio, λ, inlet conditions resulting in a stable flame are shown in Fig. 4. Burner B, with a graded pore diameter profile, has a significantly wider range of stable operating conditions. The maximum limit for stability, after which an increase in inlet velocity would result in blow-off, increases with decreasing λ. The minimum limit, however, is the same for the range of λ tested. The graded porosity burner, Burner A, was only stable at $\lambda = 1.67$, since at leaner conditions, the flame would either extinguish or blow off, and at richer conditions, the flame would flash back. However, Burner A had a 80% higher blow-off limit at $\lambda = 1.67$, as compared to Burner B.

Burners A and B each isolate the effects of the matrix-pore diameter and porosity on the flame stability performance. Although both burners have the same average pore diameter and porosity, the flame behavior is significantly affected by the difference in local properties. The smaller pore diameter region in Burner B inhibits flashback, while facilitating sufficient preheating to delay blow-off at higher velocity conditions.

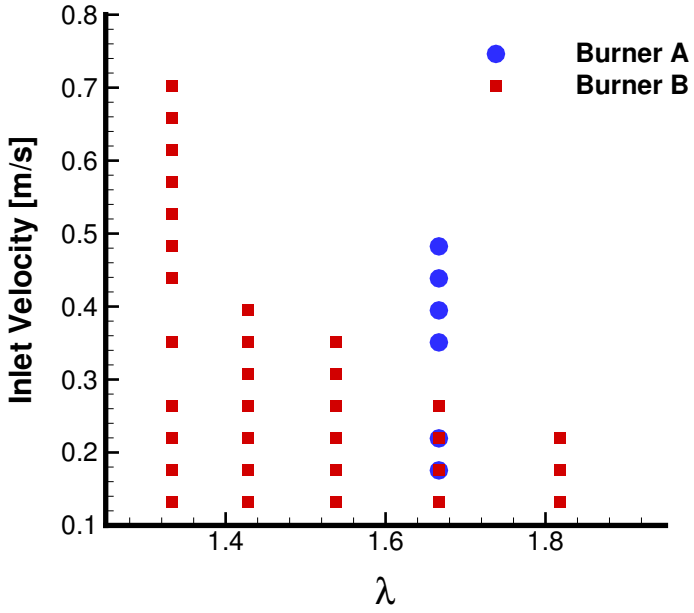

Figure 4: Experimental flame stability measurements, illustrating maximum and minimum stable velocity at each air-fuel equivalence ratio, λ, tested in Burner A and B (see Table 1).

5. Conclusions

In the present work, the feasibility of application-tailored PMBs is demonstrated using Triply Periodic Minimal Surfaces to design the porous structure and lithography-based AM for fabrication. Three-dimensional structures with specified axial porosity and pore diameter profiles were translated from computer models into physical samples, which were then tested in PMB combustion experiments. Results from these experiments show a wide range of stable operating conditions in AM ceramic porous media, depending on the geometric profile implemented. Previous experimental studies of PMBs implemented conventionally manufactured porous foams, limiting the study of the isolated effects of topology gradation, porosity distribution, and pore diameter profiles on the burner performance. The current study is an example of how the matrix topology can be tailored to achieve drastically different burner performance. As illustrated in this work, recent advances in AM for ceramics enable the design and manufacture of fully tailored PMBs, both to improve the fundamental understanding of combustion in porous media and to create application-specific designs. Future work will aim to characterize the thermal and mechanical properties of LCM-alumina implemented in the burner, and to investigate the effects of combustion on the material.

6. Acknowledgements

This work is supported by a Leading Edge Aeronautics Research for NASA (LEARN) grant (No. NNX15AE42A) and by the National Science Foundation (Award No. CBET-1800906 and Graduate Research Fellowship with No. 1656518).

References

[1] J. Binner, "Ceramics Foams", in: Cellular Ceramics, John Wiley & Sons, Ltd, 2006, chap. 2.1, pp. 31–56, DOI: 10.1002/3527606696.ch2a.

[2] D. Trimis and F. Durst, Combustion in a porous medium-advances and applications, Combustion Science and Technology 121 (1996) 153–168.

[3] S. Sobhani, D. Mohaddes, E. Boigne, P. Muhunthan, and M. Ihme, Modulation of heat transfer for extended flame stabilization in porous media burners via topology gradation, Proceedings of the Combustion Institute 37 (2019) 5697–5704.

[4] M. Schwentenwein and J. Homa, Additive manufacturing of dense alumina ceramics, International Journal of Applied Ceramic Technology 12 (2015) 1–7.

[5] G. Mitteramskogler, R. Gmeiner, R. Felzmann, S. Gruber, C. Hofstetter, J. Stampfl, J. Ebert, W. Wachter, and J. Laubersheimer, Light curing strategies for lithography-based additive manufacturing of customized ceramics, Additive Manufacturing 1-4 (2014) 110–118.

[6] I. Maskery, L. Sturm, A. Aremu, A. Panesar, C. Williams, C. Tuck, R. Wildman, I. Ashcroft, and R. Hague, Insights into the mechanical properties of several triply periodic minimal surface lattice structures made by polymer additive manufacturing, Polymer 152 (2018) 62–71.

[7] S. Rajagopalan and R. A. Robb, Schwarz meets Schwann: Design and fabrication of biomorphic and durataxic tissue engineering scaffolds, Medical Image Analysis 10 (2006) 693–712.

[8] F. P. Melchels, K. Bertoldi, R. Gabbrielli, A. H. Velders, J. Feijen, and D. W. Grijpma, Mathematically defined tissue engineering scaffold architectures prepared by stereolithography, Biomaterials 31 (2010) 6909–6916.

[9] R. Gabbrielli, I. Turner, and C. R. Bowen, Development of modelling methods for materials to be used as bone substitutes, Key Engineering Materials (2008), pp. 903–906.

[10] S. Vijayavenkataraman, L. Zhang, S. Zhang, J. Y. Hsi Fuh, and W. F. Lu, Triply periodic minimal surfaces sheet scaffolds for tissue engineering applications: An optimization approach toward biomimetic scaffold design, ACS Applied Bio Materials 1 (2018) 259–269.

[11] H. A. Schwarz, Gesammelte mathematische Abhandlungen, vol. 1, J. Springer, 1890.

[12] A. H. Schoen, Infinite periodic minimal surfaces without self-intersections, (1970).